




BRIEF DEFINITIVE REPORT

Caspase-11 auto-proteolysis is crucial for noncanonical inflammasome activation

Bettina L. Lee^{1*}, Irma B. Stowe^{1*}, Aaron Gupta¹, Opher S. Kornfeld¹, Merone Roose-Girma², Keith Anderson², Søren Warming² , Juan Zhang³, Wyne P. Lee³ , and Nobuhiko Kayagaki¹ 

Intracellular LPS sensing by caspase-4/5/11 triggers proteolytic activation of pore-forming gasdermin D (GSDMD), leading to pyroptotic cell death in Gram-negative bacteria-infected cells. Involvement of caspase-4/5/11 and GSDMD in inflammatory responses, such as lethal sepsis, makes them highly desirable drug targets. Using knock-in (KI) mouse strains, we herein provide genetic evidence to show that caspase-11 auto-cleavage at the inter-subunit linker is essential for optimal catalytic activity and subsequent proteolytic cleavage of GSDMD. Macrophages from caspase-11-processing dead KI mice (*Casp11^{PrC} D285A/D285A*) exhibit defective caspase-11 auto-processing and phenocopy *Casp11^{-/-}* and caspase-11 enzymatically dead KI (*Casp11^{Enz} C254A/C254A*) macrophages in attenuating responses to cytoplasmic LPS or Gram-negative bacteria infection. *Gsdmd^{D276A/D276A}* KI macrophages also fail to cleave GSDMD and are hypo-responsive to inflammasome stimuli, confirming that the GSDMD Asp₂₇₆ residue is a nonredundant and indispensable site for proteolytic activation of GSDMD. Our data highlight the role of caspase-11 self-cleavage as a critical regulatory step for GSDMD processing and response against Gram-negative bacteria.

Introduction

Murine caspase-11 (caspase-4 and caspase-5 in humans) mediates noncanonical inflammasome signaling, leading to pyroptotic cell death in response to Gram-negative bacteria infection (Kayagaki et al., 2011; Broz et al., 2012; Rathinam et al., 2012; Achoui et al., 2013). Cytoplasmic LPS derived from invading Gram-negative bacteria is the pathogen-associated molecular pattern that activates caspase-11 (Hagar et al., 2013; Kayagaki et al., 2013). Mechanistically, LPS binds directly to the caspase recruitment domain (CARD) of caspase-11 and initiates oligomerization and proximity-induced activation of caspase-11 catalytic activity (Shi et al., 2014). Activated caspase-11 proteolytically cleaves gasdermin-D (GSDMD) to create a 30-kD, pore-forming GSDMD N-terminus fragment (GSDMD-NT) that can insert itself into the cell membrane to form pores. GSDMD-NT pore formation immediately causes an ionic gradient loss, leading to osmotic burst and cell membrane rupture (pyroptosis; Kayagaki et al., 2015; Shi et al., 2015; Aglietti et al., 2016; Ding et al., 2016; Liu et al., 2016; Sborgi et al., 2016). Like many bacterial pore-forming toxins (e.g., listeriolysin-O), pore-forming GSDMD-NT also triggers NLRP3 sensor-mediated caspase-1 activation, leading to proteolytic activation of proinflammatory cytokines (IL-1 β and IL-18; Meixenberger et al., 2010; Kayagaki et al., 2011, 2015). A

robust level of activated mature IL-1 β and other inflammatory intracellular danger-associated molecular patterns are passively released through the GSDMD pore and/or plasma cell membrane gaps created by a secondary osmotic burst.

Inflammatory caspases (caspase-1/4/5/11) that contain CARD domains can trigger pyroptosis through limited proteolysis of GSDMD. In addition, caspase-1 can cleave itself at multiple aspartic acid residues located at internal linkers that bridge the CARD domain, large subunit (p20), and small subunit (p10) (Thornberry et al., 1992; Walker et al., 1994; Broz et al., 2010; Guey et al., 2014). Previous studies, including Thornberry et al.'s initial discovery of caspase-1, demonstrate that a caspase-1 heterotetramer (p20/p10)₂ complex represents an enzymatically active form which efficiently cleaves pro-IL-1 β (Thornberry et al., 1992; Walker et al., 1994). Subsequently, two different groups examined the role of caspase-1 auto-processing in pyroptosis induction and IL-1 β release by using *Casp1^{-/-}* macrophages reconstituted with an auto-cleavage dead mutant form of caspase-1 (Broz et al., 2010; Guey et al., 2014). The mutant largely lost the ability to release IL-1 β , but retained capacity to induce pyroptosis in response to inflammasome stimuli. Similarly, when overexpressed, caspase-11 can cleave itself at two internal sites: (1) VFVD₅₉↓A or FSVD₈₀↓P

¹Department of Physiological Chemistry, Genentech Inc., South San Francisco, CA; ²Department of Molecular Biology, Genentech Inc., South San Francisco, CA; ³Department of Immunology, Genentech Inc., South San Francisco, CA.

*B.L. Lee and I.B. Stowe contributed equally to this paper; Correspondence to Nobuhiko Kayagaki: kayagaki.nobuhiko@gene.com.

© 2018 Genentech This article is distributed under the terms of an Attribution–Noncommercial–Share Alike–No Mirror Sites license for the first six months after the publication date (see <http://www.rupress.org/terms/>). After six months it is available under a Creative Commons License (Attribution–Noncommercial–Share Alike 4.0 International license, as described at <https://creativecommons.org/licenses/by-nc-sa/4.0/>).

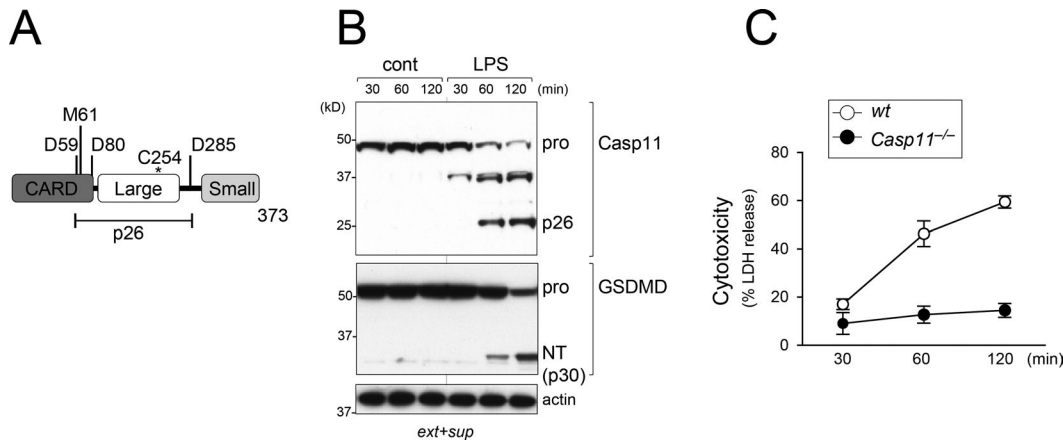


Figure 1. Induction of cleaved caspase-11 fragment in macrophages in response to cytoplasmic LPS. (A) Schematic of caspase-11 representing the CARD domain and large and small catalytic subunits. Predicted cleavage sites D59, D80, and D285 are indicated. Asterisk (*) marks critical cysteine residue in caspase-11 catalytic site (C254). M61 is a predicted alternative start site. **(B and C)** BMDMs were treated with 1 μg/ml Pam3CSK4 for 5 h before stimulation. **(B)** Immunoblot of caspase-11, GSDMD, and actin in combined cell extract (ext) and supernatant (sup) from WT BMDMs 30, 60, and 120 min after LPS electroporation or control. **(C)** LDH release time course in WT BMDMs 30, 60, and 120 min after LPS stimulation from cells in B. Data are presented as mean ± SD (n = 3) in C and representative of at least two independent experiments (B and C).

that removes the N-terminus CARD domain from the catalytic large subunit (CARD↓large subunit) and (2) MEAD₂₈₅↓A, which segregates large and small catalytic subunits (large↓small subunit; Wang et al., 1996; Kayagaki et al., 2011). Additionally, processed fragments of endogenous caspase-4/11 could be detected when cells were stimulated with LPS or infected with bacteria (Kayagaki et al., 2011; Casson et al., 2013, 2015; Kajiwara et al., 2014; Pilla et al., 2014). However, the biological significance of caspase-11 cleavage and its role under physiological conditions remain unknown.

Results and discussion

Induction of cleaved caspase-11 fragment in macrophages in response to cytoplasmic LPS

We and others have previously reported the appearance of a large caspase-11 subunit p26 fragment released into cell culture supernatant of bone marrow-derived macrophages (BMDMs) following noncanonical inflammasome stimulation (Fig. 1 A; Kayagaki et al., 2011; Casson et al., 2013; Pilla et al., 2014). In contrast, other groups have observed caspase-11 activation and pyroptosis without detectable levels of cleaved caspase-11 (Hagar et al., 2013; Yang et al., 2015). To optimize conditions to better detect cleaved caspase-11, we initially examined the induction of caspase-11 processing in a time course study. BMDMs were electroporated with LPS to rapidly engage noncanonical inflammasome activation and incubated with low volumes of media to increase sensitivity of detection. Cells were lysed and combined with supernatant, then run directly on SDS-PAGE without the need for any secondary protein concentration steps or immunoprecipitation. Combined cell extracts and supernatant were examined to focus exclusively on caspase-11 processing rather than cell death or the subsequent release of fragments into the supernatant. Using our optimized method, we could readily visualize the induction of caspase-11 processing, which was supported by the appearance of the large subunit p26 fragment (Fig. 1 B). The processed

caspase-11 p26 fragment appeared 60 min after LPS stimulation in WT macrophages. Accordingly, the appearance of caspase-11 p26 was concomitant with a reduction in pro-caspase-11 levels. Following activation, caspase-11 enzymatically cleaves GSDMD at Asp₂₇₆ to release the GSDMD-NT pore-forming fragment (Kayagaki et al., 2015; Shi et al., 2015). In agreement with this model, induction of caspase-11 p26 processing was concurrent with the appearance of GSDMD-NT (p30) and pyroptotic death, as shown by immunoblots of extract + supernatant and lactate dehydrogenase (LDH) release into cell culture supernatant, respectively (Fig. 1, B and C). These results confirm that caspase-11 is processed into a caspase-11 p26 fragment in BMDMs undergoing pyroptosis. Besides caspase-11 p26, another band appeared around 38 kD upon LPS stimulation (Fig. 1 B). The appearance of this ~38-kD caspase-11 band may represent a previously reported transcriptionally induced pro-caspase-11 isoform (M₆₁-N₃₇₃; Wang et al., 1996; Kayagaki et al., 2011) or a partially processed fragment of caspase-11 (e.g. M₁-D₂₈₅ CARD large subunit or A₆₀-N₃₇₃ large-small subunit; Fig. 1 A).

Caspase-11 auto-processing at Asp₂₈₅ is essential for GSDMD processing, pyroptosis, and IL-1β release

To better understand the roles of enzymatic activity and processing of caspase-11, we established mutant knock-in (KI) mouse lines in C57BL/6N using CRISPR/Cas9 technology. To assess the contribution of caspase-11 enzymatic activity, we mutated the critical cysteine at position 254 to an alanine to generate an enzymatically inactive caspase-11 KI mouse (Casp11^{Enz C254A/C254A}). Additionally, to highlight the role of caspase-11 processing, we generated a mouse harboring an aspartic acid to alanine mutation at position 285 (Casp11^{PrC D285A/D285A}) to disrupt the processing site in the linker region between the large and small subunits of caspase-11 (Wang et al., 1996; large↓small subunit, Fig. 1 A). Both newly founded mutant mouse lines, Casp11^{Enz C254A/C254A} and Casp11^{PrC D285A/D285A}, exhibited normal development, viability, and fertility, suggesting that blocking caspase-4/11 activation in vivo is not deleterious.

WT and *Casp11^{Prc D285A/D285A}* BMDMs were confirmed to express comparable protein levels of caspase-11, while *Casp11^{Enz C254A/C254A}* BMDMs expressed slightly higher levels of pro-caspase-11 (Fig. S1 A). Upon overexpression in HEK293 cells, caspase-11 can itself become a substrate and auto-cleave at VFVD₅₉↓A (or FSVD₈₀↓P) and MEAD₂₈₅↓A to generate a large p26 subunit and small subunit (Fig. 1 A; Wang et al., 1996). Consistent with this overexpression study, *Casp11^{Enz C254A/C254A}* BMDMs failed to generate a caspase-11 p26 fragment (Fig. 2 A). Likewise, induction of caspase-11 p26 was absent in *Casp11^{Prc D285A/D285A}* BMDMs. These data corroborate the existence of a detectable caspase-11 self-cleaved fragment generated by proteolytic processing at a nonredundant residue (Asp₂₈₅) within the inter-subunit linker. Furthermore, conserved P₁ and P₁' residues in human caspase-4 (LEED₂₈₉↓A) and other species suggest there is an evolutionarily conserved mechanism for caspase-4/11 auto-proteolysis (Fig. S1 B).

To determine the importance of caspase-11 auto-processing in pyroptosis induction, we next examined the proteolytic activation of a direct substrate of caspase-11, GSDMD. Similar to *Casp11^{-/-}* BMDMs, *Casp11^{Enz C254A/C254A}* and *Casp11^{Prc D285A/D285A}* BMDMs failed to generate a GSDMD-NT fragment (Fig. 2 A). Since creation of GSDMD-NT is necessary for pyroptosis (Kayagaki et al., 2015; Shi et al., 2015), we next assayed for the occurrence of pyroptosis by monitoring plasma membrane integrity through imaging and LDH release. The failure of *Casp11^{Enz C254A/C254A}* and *Casp11^{Prc D285A/D285A}* BMDMs to respond to LPS was confirmed by live-cell imaging using a cell-impermeable fluorescent dye (YOYO-1) that marks dying cells with damaged plasma cell membranes (Fig. 2 B). Accordingly, *Casp11^{-/-}*, *Casp11^{Enz C254A/C254A}*, and *Casp11^{Prc D285A/D285A}* BMDMs were similarly unresponsive to cytoplasmic LPS as measured by LDH release, while retaining normal responses to NLRP3 (ATP and nigericin)- or NLRC4 (flagellin)-dependent canonical inflammasome activation (Mariathasan et al., 2006; Sutterwala et al., 2007) (Fig. 2 C and Fig. S1 C). These data clearly show that caspase-11 processing at Asp₂₈₅ is functionally required for LPS-mediated GSDMD cleavage and pyroptosis.

Beyond pyroptosis, the pore-forming GSDMD-NT can also lead to noncanonical activation of the NLRP3 inflammasome, resulting in caspase-1-dependent activation and release of the proinflammatory cytokines, IL-1 β and IL-18 (Kayagaki et al., 2011, 2015). Mutating caspase-11 at either the active catalytic site (Cys₂₅₄) or auto-cleavage site (Asp₂₈₅) significantly reduced levels of proinflammatory cytokines released from cytoplasmic LPS-stimulated BMDMs (Fig. 2 C). These results are consistent with the attenuated GSDMD-NT formation seen in *Casp11^{Enz C254A/C254A}* and *Casp11^{Prc D285A/D285A}* BMDMs (Fig. 2 A). Furthermore, this defect is specific to LPS-dependent responses, as IL-1 β and IL-18 levels released upon NLRP3 canonical stimuli remained unchanged (Fig. 2 C and Fig. S1 C).

To examine responses in the context of bacterial infections, we exposed BMDMs to Gram-negative bacteria (*Escherichia coli*, *Shigella flexneri*, and *Citrobacter rodentium*), which activate the caspase-11-dependent inflammasome (Kayagaki et al., 2011; Rathinam et al., 2012). We found that both *Casp11^{Enz C254A/C254A}* and *Casp11^{Prc D285A/D285A}* BMDMs phenocopied *Casp11^{-/-}* BMDMs by failing to secrete proinflammatory cytokines or undergo pyroptosis upon Gram-negative bacteria infection. However, they

continue to respond to the canonical inflammasome (NLRC4) triggered by *Pseudomonas aeruginosa* infection (Fig. 2 D; Sutterwala et al., 2007).

We also confirmed that mutating caspase-11 at the processing site (Asp₂₈₅) is unlikely to cause improper folding or result in dysfunction beyond disruption of auto-cleavage. Homology modeling of caspase-11 using the caspase-1 x-ray crystal structure (Elliott et al., 2009) shows Asp₂₈₅ is located in a thermally flexible linker region of caspase-11 (Fig. S1 D). Additionally, WT and D285A mutant caspase-11 bound LPS equivalently in a biotin-LPS pull-down study, confirming D285A replacement does not impair the caspase-11 CARD-LPS interaction (Fig. S1 E; Shi et al., 2014). Furthermore, when caspase-11 auto-processing was mimicked by coexpressing large and small catalytic subunits as separate constructs in HEK293T cells, both WT and D285A mutant versions showed comparable proteolytic activity as measured by GSDMD processing (Fig. S1 F).

Collectively, we provide strong genetic evidence highlighting the requirement of caspase-11 auto-processing at the inter-subunit linker for its optimal activation. Auto-proteolysis at the inter-subunit linker (large↓small subunit) mediates downstream GSDMD cleavage, rapid execution of pyroptosis, and proinflammatory cytokine release. The physiological role of cleavage at Asp₅₉ or Asp₈₀ (CARD↓large subunit), however, remains unclear. In the case of caspase-1, CARD↓large subunit auto-cleavage can create a p20/p10 complex that is catalytically active (Thornberry et al., 1992), yet has also been reported to be relatively unstable (Walsh et al., 2011; Boucher et al., 2018).

GSDMD Asp₂₇₆ residue is the critical nonredundant cleavage site following caspase-1/11 activation

In a cell-free system using recombinant proteins, pro-GSDMD can be directly cleaved by caspase-1/11 at LLSD₂₇₆↓G (FLTD₂₇₅↓G in human; Agard et al., 2010; Kayagaki et al., 2015; Shi et al., 2015), an essential step in the creation of pore-forming GSDMD-NT. To genetically validate this model, we generated a mutant KI mouse (*Gsdmd^{D276A/D276A}*) with an alanine replacing the aspartic acid at position 276. Our previous study used immortalized macrophages reconstituted with overexpressed GSDMD to demonstrate that the Asp₂₇₆ to Ala mutation can abrogate processing in response to cytoplasmic LPS (Kayagaki et al., 2015). Consistently, GSDMD-NT was undetectable in *Gsdmd^{D276A/D276A}* BMDMs after stimulation with cytoplasmic LPS (Fig. 3 A), confirming that LLSD₂₇₆↓G is a nonredundant cleavage site for caspase-11. When *Gsdmd^{D276A/D276A}* BMDMs were stimulated with ATP to activate the caspase-1 canonical inflammasome, we did not observe the 30-kD GSDMD-NT, but rather an aberrant 43-kD GSDMD fragment (Fig. 3 A and Fig. S2). This band seems to represent a previously reported nonfunctional GSDMD C-terminus p43 fragment that is aberrantly generated by caspase-3 cleavage at aspartic acid position 87 (Asp₈₇; Fig. S2; Taabazuing et al., 2017). Accordingly, caspase-3 activation can be induced by caspase-1 in macrophages upon canonical inflammasome stimuli, although its physiological relevance remains unclear (Van de Craen et al., 1999; Sagulenko et al., 2018). It is unlikely that caspase-1 directly cleaves GSDMD at Asp₈₇ since aberrant GSDMD C-terminus p43 does not appear when GSDMD is incubated with recombinant caspase-1 (Agard et al., 2010; Ramirez et al., 2018).

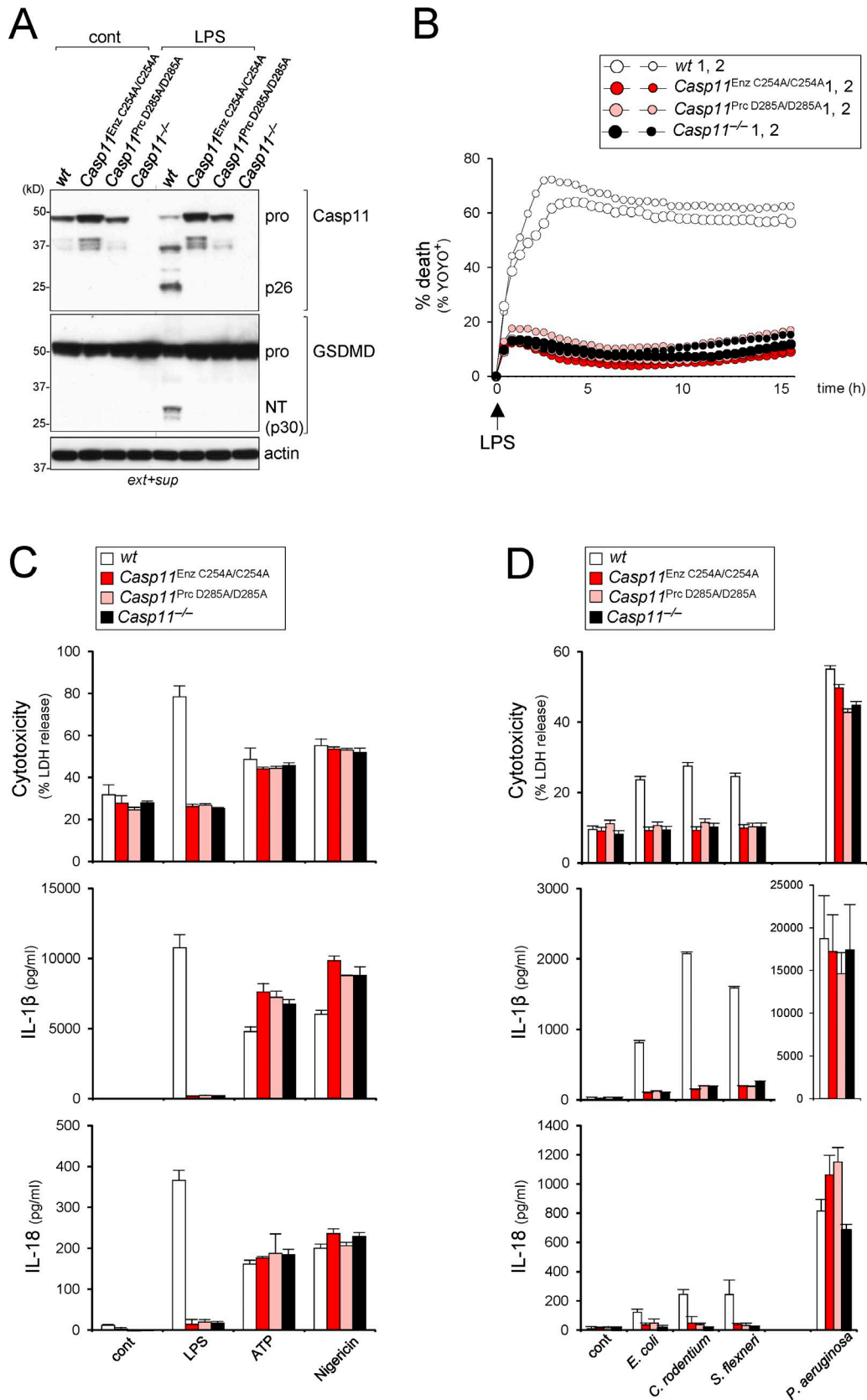


Figure 2. **Caspase-11 auto-processing at Asp₂₈₅ is essential for GSDMD processing, pyroptosis, and IL-1β release.** (A–D) BMDMs were treated with 1 μg/ml Pam3CSK4 for 5 h. (A) Immunoblot of caspase-11, GSDMD, and actin in extract (ext) + supernatant (sup) from WT, *Casp11^{Enz C254A/C254A}*, and *Casp11^{Prc D285A/D285A}* BMDMs at 60 min after LPS electroporation or control. (B) Cell death measured by percent YOYO-1⁺ cells from live cell images taken every 30 min over a 16-h time course following LPS electroporation of BMDMs from two mice per genotype. (C) LDH, IL-1β, and IL-18 release from BMDMs

Functionally, BMDMs from *Gsdmd*^{D276A/D276A} mice were defective in pyroptosis and proinflammatory cytokine release following cytoplasmic LPS stimulation, similar to *Gsdmd*^{-/-} (Fig. 3, B and C). Caspase-1 relies exclusively on GSDMD to execute pyroptosis at early time points (Kayagaki et al., 2015; Shi et al., 2015). When BMDMs were stimulated with canonical inflammasome stimuli (ATP or nigericin) to activate caspase-1, *Gsdmd*^{D276A/D276A} BMDMs again phenocopied *Gsdmd*^{-/-} by exhibiting attenuated release of LDH, IL-1 β , and IL-18 (3-h ATP and 30-min nigericin time points; Fig. 3 C). These results are consistent with the aberrant GSDMD C-terminus p43 representing a nonfunctional fragment (Taabazuing et al., 2017). We next determined whether processing at Asp₂₇₆ was important under conditions with bacterial infection. *Gsdmd*^{D276A/D276A} BMDMs were unresponsive to Gram-negative *C. rodentium* (noncanonical inflammasome) or *P. aeruginosa* (canonical inflammasome), as previously shown for *Gsdmd*^{-/-} (Fig. 3 D). Together these data provide genetic evidence confirming that Asp₂₇₆ is the physiological nonredundant cleavage site in GSDMD, and cleavage at this site is the final trigger to initiate pyroptosis.

Caspase-11 auto-processing and GSDMD cleavage are required to induce acute septic shock

To further investigate the role of caspase-11 catalytic activity and auto-processing in vivo, we challenged mice with a high dose of LPS, which is a model of acute septic shock dependent on caspase-11 and GSDMD-mediated pyroptosis (Wang et al., 1998; Kayagaki et al., 2011, 2015). Similar to *Casp11*^{-/-} mice, both *Casp11*^{Enz C254A/C254A} and *Casp11*^{PrC D285A/D285A} were resistant to LPS-induced lethal septic shock (Fig. 4 A and Fig. S3 A). Intraperitoneal injection of LPS is also known to increase serum levels of IL-1 β and IL-18 cytokines through the caspase-11-dependent NLRP3 inflammasome pathway (Kayagaki et al., 2011). In accordance with in vitro data (Fig. 2 C), serum IL-1 β and IL-18 cytokine levels were similarly reduced in all caspase-11 mutant lines tested (Fig. 4 B). To determine if GSDMD processing was critical for resistance to acute septic shock, we also challenged *Gsdmd*^{D276A/D276A} mice to high doses of LPS. Similar to *Gsdmd*^{-/-} mice, *Gsdmd*^{D276A/D276A} mice displayed marked resistance to LPS challenge, whereas WT mice succumbed within 24 h (Fig. 4 C and Fig. S3 B). Collectively, these in vivo data highlight the crucial roles of caspase-11 catalytic activity, caspase-11 auto-processing, and GSDMD cleavage in lethal septic shock.

Recent emerging reports have established a paradigm in which a single cut at GSDMD-Asp₂₇₆ by caspase-1/4/5/11 can instantly perforate the cell membrane and result in pyroptotic cell death (Kayagaki et al., 2015; Shi et al., 2015). Our studies with *Gsdmd*^{D276A/D276A} mice provide the first genetic evidence that cleavage at Asp₂₇₆, between the pore-forming GSDMD-NT and the self-inhibitory C-terminus, is a critical and nonredundant step in the execution of an inducible pyroptotic program. Furthermore, our studies with *Casp11*^{Enz C254A/C254A} and *Casp11*^{PrC D285A/D285A} mice genetically validate the hypothesis that an additional proteolytic

step (caspase-11 auto-processing) precedes GSDMD cleavage. This self-proteolysis step is essential for all downstream events, including GSDMD activation, IL-1 β and IL-18 release, and lethal sepsis induction, thus refining the model for noncanonical inflammasome activation.

Auto-proteolysis for optimal caspase activation is not without precedent. Caspase-8 auto-processing has been shown to be an important event for apoptosis in studies using gene targeted KI mice or bacterial artificial chromosome transgenic mice that harbor a caspase-8 auto-processing dead mutant (Kang et al., 2008; Philip et al., 2016). Caspase-1, another initiator caspase, is also auto-processed in response to canonical inflammasome stimuli. *Casp1*^{-/-} macrophages reconstituted with caspase-1-processing dead mutants reportedly attenuate IL-1 β release, but retain the ability to undergo caspase-1-dependent pyroptosis (Broz et al., 2010; Guey et al., 2014). However, it should be noted that the ability of caspase-1-processing dead mutant cells to induce cell death does not necessarily correlate with intact GSDMD cleavage. Caspase-1 is known to engage GSDMD-independent pyroptosis in *Gsdmd*^{-/-} macrophages (Kayagaki et al., 2015), and GSDMD-NT induction was not examined in the reconstituted cells (Broz et al., 2010; Guey et al., 2014). Additional studies with primary cells from caspase-1 auto-processing dead mutant KI mice are needed to better understand the role of caspase-1 auto-processing in GSDMD activation and pyroptosis induction at physiological settings.

Although the exact mechanism for the initial caspase-11 activation step remains unclear, it likely mirrors the proximity-induced dimerization model reported for initiator apoptotic caspases (Renatus et al., 2001; Boatright and Salvesen, 2003). The lipid A moiety of LPS binds directly to the caspase-11 CARD domain and leads to the oligomerization and proximity-induced activation of caspase-11 (Shi et al., 2014), an event likely due to the aggregation behavior of LPS. LPS-induced proximity initiates two sequential steps for activation: (1) pro-caspase-11 gains limited catalytic activity which (2) triggers large \downarrow small subunit auto-processing to create a heterotetramer complex ([large subunit p26/small subunit]₂ or [CARD large subunit/small subunit]₂) with optimal catalytic activity. This fine-tuned activation through large \downarrow small subunit self-cleavage is a crucial event for GSDMD conversion into its active pore-forming GSDMD-NT fragment. By requiring a caspase-11 auto-processing step before undergoing pyroptosis, macrophages have imposed an intrinsic safety mechanism to prevent excess or unwarranted induction of pyroptosis.

It has been hypothesized that caspase-11 is activated in the cytosol following Gram-negative bacterial infection (Aachoui et al., 2013; Case et al., 2013). An as yet to be developed probe that can specifically detect cleaved caspase-4/11 will be a helpful tool in understanding the exact location where caspase-4/11 is activated. Our genetic studies definitively demonstrate that cleaved caspase-4/11 and cleaved GSDMD represent candidate markers for detection of pyroptotic cells in vivo.

stimulated with transfected LPS (5 μ g/ml plus FuGENE HD), ATP (5 mM), or nigericin (10 μ g/ml) after 16 h, 3 h, or 30 min, respectively. (D) LDH, IL-1 β , and IL-18 release measured from supernatants of BMDMs infected with indicated strains of bacteria. Data are representative of at least two independent experiments (A and B). Data are presented as mean \pm SD ($n = 3$) and representative of at least three independent experiments (C and D).

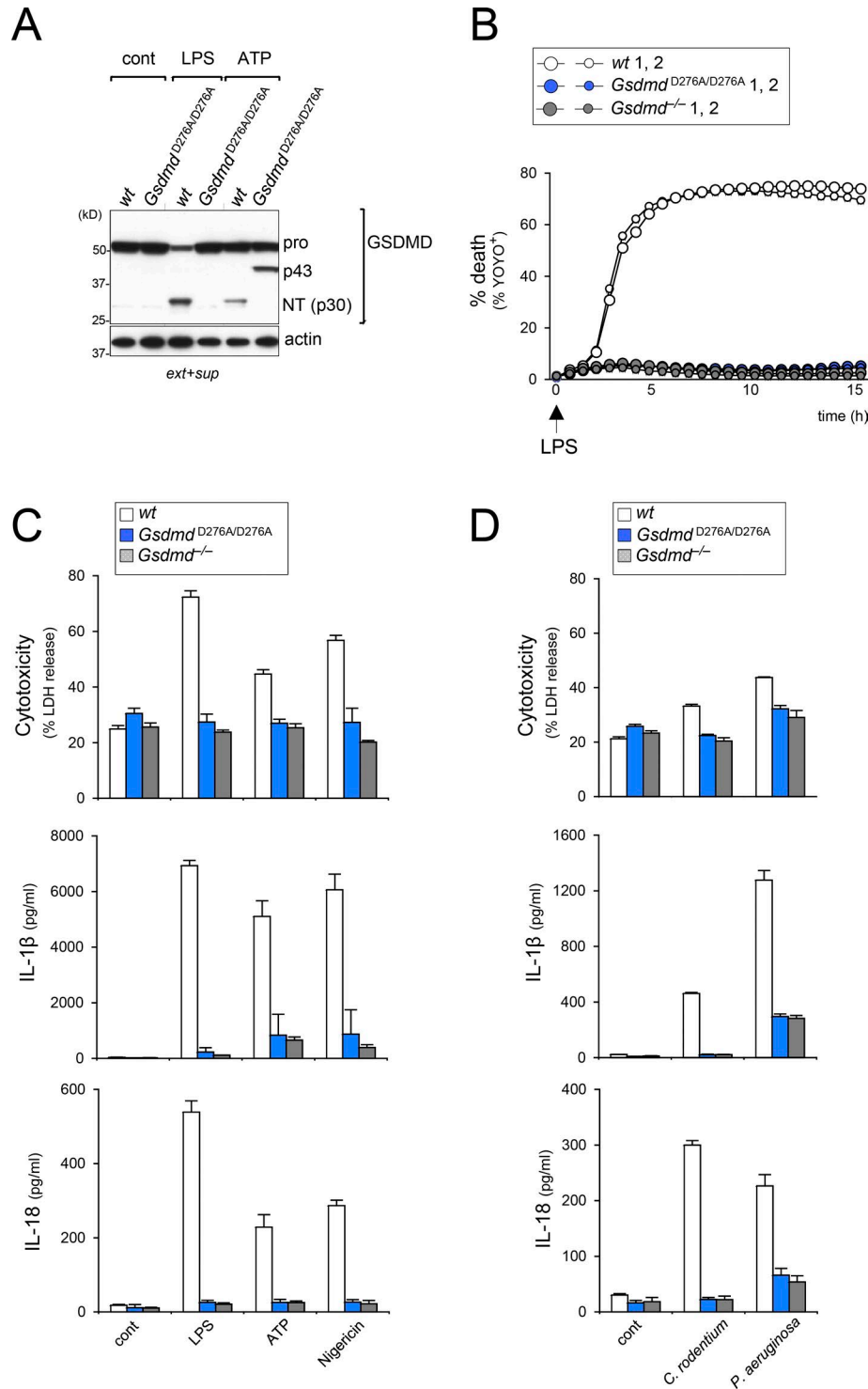


Figure 3. **GSDMD Asp₂₇₆ residue is the critical nonredundant cleavage site following caspase-1/11 activation.** (A–D) BMDMs were treated with 1 μg/ml Pam3CSK4 for 5 h before stimulation. (A) Immunoblot of GSDMD and actin in combined cell extract (ext) + supernatant (sup) from WT and *Gsdmd*^{D276A/D276A} BMDMs after 60 min following control treatment, LPS electroporation, or ATP stimulation for detection of GSDMD full-length (pro), GSDMD NT (p30), and p43. (B) Cell death measured by percent YOYO-1⁺ cells from live cell images taken every 30 min over a 16 h time course following LPS electroporation of BMDMs from two mice per genotype. (C) LDH, IL-1β, and IL-18 release measured from supernatants of BMDMs stimulated with transfected LPS (5 μg/ml plus FuGENE HD), ATP (5 mM), or nigericin (10 μg/ml) after 16 h, 3 h, or 30 min, respectively. (D) LDH, IL-1β, and IL-18 release measured from supernatants of BMDMs infected with indicated strains of bacteria. Data are representative of at least two independent experiments (A and B). Data are presented as mean ± SD (n = 3) and representative of at least three independent experiments (C and D).

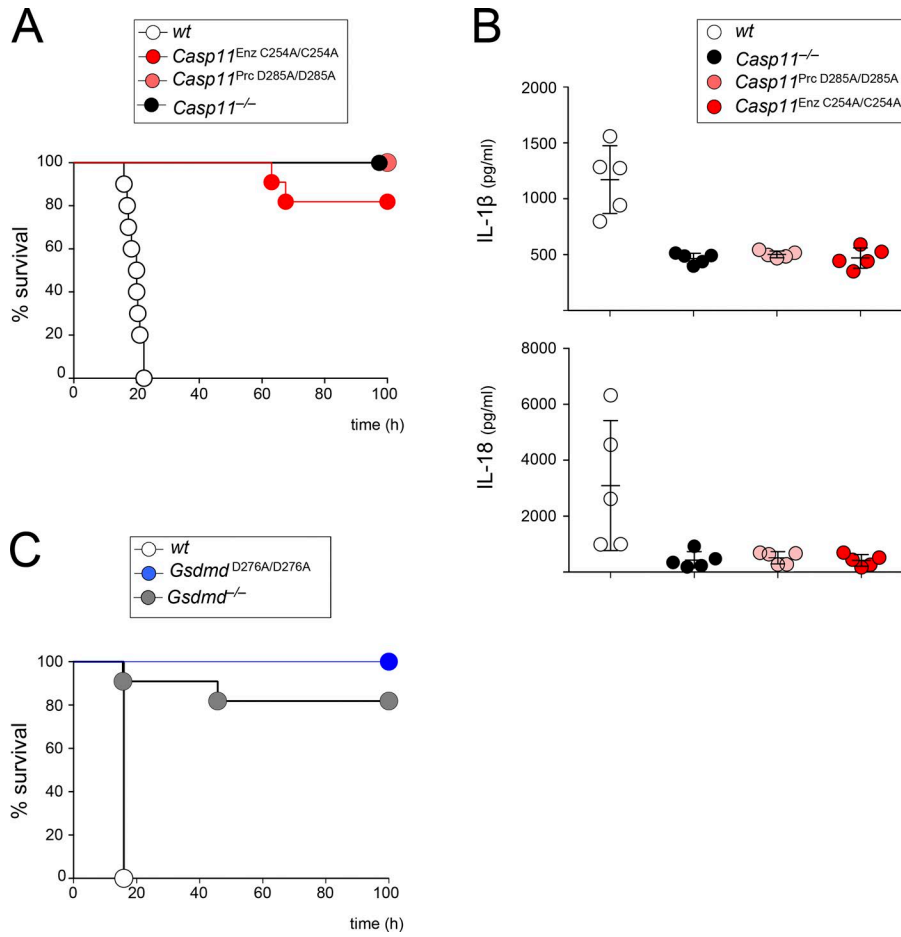


Figure 4. Caspase-11 auto-processing and GSDMD cleavage are required to induce acute septic shock. (A and C) Kaplan-Meier survival plots for mice ($n = 10$ per genotype) challenged with 54 mg/kg LPS. Adjusted P values are supplied in Figs. S3 (A and B). **(B)** Serum IL-1 β and IL-18 levels 12 h after intraperitoneal injection with 20 mg/kg LPS. Each dot represents a single animal ($n = 5$); error bars represent mean \pm SD. Data are representative of at least two independent experiments.

Materials and methods

Mice

Casp11^{-/-} (Kayagaki et al., 2011) and *Gsdmd*^{-/-} (1,632-bp deletion; Kayagaki et al., 2015) mice on a C57BL/6N background were described previously. C57BL/6N mice were purchased from Charles River Laboratories and used as WT controls for all studies. *Casp11*^{PrC D285A/D285A} mice were generated at Taconic Biosciences/Genentech from gene-targeted C57BL/6N Tac ES cells. *Casp11*^{PrC D285A/D285A} mice were genotyped with PCR primers (5'-CCAGTTGTGCAGAGGTGTAGATCT-3' and 5'-TCTCCACGTGGC TCAGCTT-3') and probes (5'-FAM/ATGGA+AGCT/ZEN/GCC GC+TGT/3IABkFQ and 5'-HEX/ATG+GAA+GCT/ZEN/G+AT+GC +TGTC/3IABkFQ). *Casp11*^{Enz C254A/C254A} mice and *Gsdmd*^{D276A/D276A} mice were obtained by pronuclear or cytoplasmic injection, respectively, of C57BL/6N zygotes with 25 ng/ μ l WT Cas9 mRNA (Thermo Fisher), 13 ng/ μ l single-guide RNA prepared by MEGAs-hortscript T7 kit (Thermo Fisher), and 100 ng/ μ l donor template (PAGE-purified Ultramer, Integrated DNA Technologies). Tail DNA from resulting G0 mosaic offspring was analyzed by PCR followed by Sanger sequencing (*Casp11* C254A) including top-5 predicted off-target loci or droplet digital PCR and deep sequencing (*Gsdmd* D276A) for target and off-target mutations (top 15 predicted sites). G0 founders carrying the intended mutation and no off-targets were bred with WT C57BL/6N mice to generate G1 heterozygous mice. Sequences of single-guide RNA and donor oligos used are provided in Fig. S3 C. *Casp11*^{Enz C254A/C254A} mice were genotyped

with PCR primers (5'-CAGACATCAGACAGCACATTC and 5'-AGC AGCGTGGGAGTTC-3') and probes (5'-FAM/CACCTCTCGCGG CCT/MGBNFQ-3' and 5'-VIC/CACCTCTGCAGGCCT/MGBNFQ-3'). *Gsdmd*^{D276A/D276A} mice were genotyped with PCR primers (5'-CCA GCAGGTAGAAGATAGG-3', 5'-FAM/CCTCCAGATGGGATTGATG-3', and 5'-FAM/CCAGCGGGCATTGAT-3'). The Genentech Institutional Animal Care and Use Committee approved all animal studies.

Antibodies and reagents

Antibodies used include mouse GSDMD (17G2G9; Genentech; Aglietti et al., 2016), caspase-11 (clone 17D9; Novus Biologicals), Myc (Novus Biologicals), FLAG (M2; Sigma-Aldrich), and actin (AC15; Novus Biologicals). Pam3CSK4, ultra-pure LPS (*E. coli* O111:B4), ultra-pure flagellin (*P. aeruginosa*), and nigericin were purchased from Invivogen. ATP was purchased from Sigma-Aldrich, YOYO-1 dye from Thermo Fisher Scientific, and Nuclear-ID DNA stain from Enzo Life Sciences.

Immunoblot

For immunoblotting (extract + supernatant) after stimulations, 5×10^6 cells were prestimulated with 1 μ g/ml Pam3CSK4 for 5 h on plates and electroporated with 0.5–5 μ g/ml LPS in 100 μ l R buffer using Neon (Life Technologies) 100 μ l Tip with 1,720 Voltage, 10 Width, 2 Pulse settings. Electroporated cells were added to 200 μ l Opti-MEM I media (Gibco) to make a total of 300 μ l. For ATP stimulation, 5×10^6 cells were prestimulated with 1

μg/ml Pam3CSK4 (as described above), then resuspended with 5 mM ATP in 300 μl Opti-MEM I media. Cells were then split into separate tubes (70 μl/tube) and incubated for indicated times. Samples were harvested by pelleting cells and transferring supernatant to a separate tube with 1× Complete Protease Inhibitor (Roche Applied Science) added to supernatant. Remaining cells were lysed in 40 μl of radioimmunoprecipitation assay (RIPA) buffer (50 mM Tris-HCl, pH 7.4, 150 mM NaCl, 1 mM EDTA, 1× Complete Protease Inhibitor, 1% Triton X-100, 0.1% SDS). Cell extracts were then combined with supernatant for immunoblotting. For LDH and cytokine measurement of samples for immunoblot, 8 μl of stimulated cells (~100,000 cells) from the 300 μl Opti-MEM I cell mix (before lysing) were added to 200 μl of Opti-MEM I in a 96-well tissue culture plate to be imaged and collected. For all other immunoblots, 1.0×10^5 cells were directly lysed in RIPA buffer and run as whole cell lysate.

Macrophage cell culture and stimulations

Bone marrow cells were differentiated into macrophages in DMEM with 10% low endotoxin FBS (Omega Scientific) and 20% L929-conditioned medium for 5–6 d, then plated at $\sim 1.0 \times 10^6$ cells/ml with 100 μl 10%FBS/DMEM in 96-well plates and cultured overnight. For stimulations, cells were prestimulated with 1 μg/ml Pam3CSK4 for 5 h where indicated and then cultured in Opti-MEM I media with indicated stimulations, 5 mM ATP, 5 μg/ml LPS plus 0.25% vol/vol FuGENE HD (Promega; [Kayagaki et al., 2013](#)), nigericin 10 μg/ml, or subjected to Neon electroporations. For IncuCyte imaging analysis, the Neon transfection system was used with 1,720 voltage, 10 width, 2 pulse settings and performed with 5×10^6 cells plus 0.5–5 μg/ml LPS and plated at 10^5 cells/200 μl Opti-MEM I with 200 nM YOYO-1 per 96-well. For AMAXA electroporation, 500 ng/ml flagellin or 5 μg/ml LPS were electroporated into $\sim 5.0 \times 10^5$ cells in Opti-MEM I media 24-well plates using the AMAXA 4D-Nucleofector system Y-unit (Lonza). Infections with *P. aeruginosa* (ATCC 27853; multiplicity of infection [moi] 25), *E. coli* (ATCC 11775, moi 30), *C. rodentium* (ATCC 51116, moi 20), or *S. flexneri* (ATCC 9199, moi 20) were for 1.5 h and then cultures were supplemented with 100 μg/ml Gentamycin (Life Technologies). Supernatants for ATP were collected after 3 h, nigericin collected after 30 min, and *P. aeruginosa* infection collected after 3 h. All other supernatants were collected after overnight incubation unless otherwise noted.

Cell death and cytokine measurements

LDH release was measured using CytoTox 96 Non-Radioactive Cytotoxicity Assay (Promega) according to manufacturer's instructions. Data calculated as percent death (signal over max death after treatment with 0.1% Triton). YOYO-1 (491/509) dye (at 200 nM final concentration) was added at the time of stimulation and scanned in green channel every 30 min to 1 h for at least 16 h on the Essen BioScience IncuCyte ZOOM at 10× magnification. Nuclear-ID was added at the last time point and scanned in red channel. IncuCyte software was used to determine total number of dead YOYO⁺ cells and Nuclear-ID⁺ (live and dead). Percent death (or percent YOYO⁺) was calculated as the number of YOYO⁺ cells divided by the total number of Nuclear-ID⁺ cells. IL-1β was measured from cell culture supernatants and serum by mouse IL-1β tissue culture kit (Meso

Scale Discovery). IL-18 was measured from cell culture supernatants and serum using mouse IL-18 ELISA (MBL International).

Homology modeling

Protein structure homology modeling of caspase-11 was performed using SWISS-MODEL with caspase-1 (Protein Data Bank accession no. 3E4C) as a template ([Biasini et al., 2014](#)).

Plasmids and transient expression

cDNAs encoding N-ter 3×Myc mouse GSDMD, WT caspase-11 catalytic large subunit (A₆₀-D₂₈₅), caspase-11 D285A mutant large subunit, caspase-11 small subunit (A₂₈₆-N₃₇₃), N-ter FLAG mouse caspase-1 C284A, N-ter FLAG caspase-11 C254A, and N-ter FLAG caspase-11 C254A/D285A were synthesized and subcloned into pcDNA3.1/Zeo⁽⁺⁾ (Thermo Fisher Scientific) for transient expression in HEK293T cells. For GSDMD cleavage assay, HEK293T cells (ATCC) were cultured overnight in 96-well plates at 1.2×10^5 cells/ml, then transfected with total 60 ng of plasmid by using 0.16 μl Lipofectamine 2000 per well (Thermo Fisher Scientific). Cells were lysed with RIPA buffer + protease inhibitor cocktail (Roche Applied Science) 24 h after transfection. HEK293T cell lines used were regularly tested for mycoplasma.

Biotin-LPS pull-down assay

The biotin-LPS pull-down study was performed as previously described ([Shi et al., 2014](#)). In brief, HEK293T cells were transiently transfected with plasmids on 10-cm culture dishes using Lipofectamine 2000 according to manufacturer's instruction. 24 h after transfection, cells were lysed with Triton buffer (50 mM Tris-HCl, pH 7.6, 150 mM NaCl, 2 mM EDTA, 1% Triton X-100, protease inhibitor cocktail). LPS-binding proteins were precipitated with 1 μg of biotin-conjugated LPS (Invivogen) and Streptavidin Sepharose beads (GE Healthcare). Beads were washed three times with Triton buffer, and precipitates were eluted with 1× SDS sample buffer followed by SDS-PAGE and immunoblot analysis.

In vivo mouse studies

Female mice aged 8–10 wk were injected intraperitoneally with 54 mg/kg LPS (*E. coli* O111: B4, Sigma-Aldrich) and monitored eight times daily for a total of 6 d. Statistical analysis was performed with log-rank (Mantel-Cox) tests using Prism, and P values were adjusted to account for multiple comparisons using Bonferroni's correction. The Genentech Institutional Animal Care and Use Committee approved all animal studies.

Online supplemental material

Fig. S1 presents additional data related to [Fig. 1](#) and [Fig. 2](#) to further characterize caspase-11 mutations and corresponding KI mice. Data shows presence of caspase-11 protein in all mutants and additional evidence for defective LPS responses by caspase-11 mutants. Further data are provided to show D285A is unlikely to cause unintended dysfunction beyond disruption of caspase-11 processing. Fig. S2 is related to [Fig. 3](#) and provides a schematic of the GSDMD bands seen in [Fig. 3](#). Fig. S3 is related to [Fig. 4](#) and shows relevant P values for the data presented in [Fig. 4](#). Also included are the gRNA and donor oligo sequences related to the generation of the KI mice using CRISPR technology.

Acknowledgments

We thank Vishva M. Dixit, Kim Newton, Karen O'Rourke, Kathleen M. Mirrashidi, and Ada Ndoja for helpful discussion.

All authors are employees of Genentech, Inc., a member of the Roche group.

The authors declare no competing financial interests.

Author contributions: B.L. Lee, I.B. Stowe, A. Gupta, O.S. Kornfeld, and N. Kayagaki performed the experiments. B.L. Lee, I.B. Stowe and N. Kayagaki designed the experiments, analyzed the data, and wrote the paper. M. Roose-Girma, K. Anderson, and S. Warming made KI mice; J. Zhang and W.P. Lee performed LPS sepsis study.

Submitted: 26 March 2018

Revised: 25 June 2018

Accepted: 6 August 2018

References

- Aachoui, Y., I.A. Leaf, J.A. Hagar, M.F. Fontana, C.G. Campos, D.E. Zak, M.H. Tan, P.A. Cotter, R.E. Vance, A. Aderem, and E.A. Miao. 2013. Caspase-11 protects against bacteria that escape the vacuole. *Science*. 339:975-978. <https://doi.org/10.1126/science.1230751>
- Agard, N.J., D. Maltby, and J.A. Wells. 2010. Inflammatory stimuli regulate caspase substrate profiles. *Mol. Cell. Proteomics*. 9:880-893. <https://doi.org/10.1074/mcp.M900528-MCP200>
- Aglietti, R.A., A. Estevez, A. Gupta, M.G. Ramirez, P.S. Liu, N. Kayagaki, C. Ciferri, V.M. Dixit, and E.C. Dueber. 2016. GsdmD p30 elicited by caspase-11 during pyroptosis forms pores in membranes. *Proc. Natl. Acad. Sci. USA*. 113:7858-7863. <https://doi.org/10.1073/pnas.1607769113>
- Biasini, M., S. Bienert, A. Waterhouse, K. Arnold, G. Studer, T. Schmidt, F. Kiefer, T. Gallo Cassarino, M. Bertoni, L. Bordoli, and T. Schwede. 2014. SWISS-MODEL: modelling protein tertiary and quaternary structure using evolutionary information. *Nucleic Acids Res.* 42(W1):W252-258. <https://doi.org/10.1093/nar/gku340>
- Boatright, K.M., and G.S. Salvesen. 2003. Mechanisms of caspase activation. *Curr. Opin. Cell Biol.* 15:725-731. <https://doi.org/10.1016/j.ceb.2003.10.009>
- Boucher, D., M. Monteleone, R.C. Coll, K.W. Chen, C.M. Ross, J.L. Teo, G.A. Gomez, C.L. Holley, D. Bierschenk, K.J. Stacey, et al. 2018. Caspase-1 self-cleavage is an intrinsic mechanism to terminate inflammasome activity. *J. Exp. Med.* 215:827-840. <https://doi.org/10.1084/jem.20172222>
- Broz, P., J. von Moltke, J.W. Jones, R.E. Vance, and D.M. Monack. 2010. Differential requirement for Caspase-1 autoproteolysis in pathogen-induced cell death and cytokine processing. *Cell Host Microbe*. 8:471-483. <https://doi.org/10.1016/j.chom.2010.11.007>
- Broz, P., T. Ruby, K. Belhocine, D.M. Bouley, N. Kayagaki, V.M. Dixit, and D.M. Monack. 2012. Caspase-11 increases susceptibility to Salmonella infection in the absence of caspase-1. *Nature*. 490:288-291. <https://doi.org/10.1038/nature11419>
- Case, C.L., L.J. Kohler, J.B. Lima, T. Strowig, M.R. de Zoete, R.A. Flavell, D.S. Zamboni, and C.R. Roy. 2013. Caspase-11 stimulates rapid flagellin-independent pyroptosis in response to Legionella pneumophila. *Proc. Natl. Acad. Sci. USA*. 110:1851-1856. <https://doi.org/10.1073/pnas.1211521110>
- Casson, C.N., A.M. Copenhaver, E.E. Zwack, H.T. Nguyen, T. Strowig, B. Javdan, W.P. Bradley, T.C. Fung, R.A. Flavell, I.E. Brodsky, and S. Shin. 2013. Caspase-11 activation in response to bacterial secretion systems that access the host cytosol. *PLoS Pathog.* 9:e1003400. <https://doi.org/10.1371/journal.ppat.1003400>
- Casson, C.N., J. Yu, V.M. Reyes, F.O. Taschuk, A. Yadav, A.M. Copenhaver, H.T. Nguyen, R.G. Collman, and S. Shin. 2015. Human caspase-4 mediates noncanonical inflammasome activation against gram-negative bacterial pathogens. *Proc. Natl. Acad. Sci. USA*. 112:6688-6693. <https://doi.org/10.1073/pnas.1421699112>
- Ding, J., K. Wang, W. Liu, Y. She, Q. Sun, J. Shi, H. Sun, D.C. Wang, and F. Shao. 2016. Pore-forming activity and structural autoinhibition of the gasdermin family. *Nature*. 535:111-116. <https://doi.org/10.1038/nature18590>
- Elliott, J.M., L. Rouge, C. Wiesmann, and J.M. Scheer. 2009. Crystal structure of procaspase-1 zymogen domain reveals insight into inflammatory caspase autoactivation. *J. Biol. Chem.* 284:6546-6553. <https://doi.org/10.1074/jbc.M806121200>
- Guey, B., M. Bodnar, S.N. Manié, A. Tardivel, and V. Petrilli. 2014. Caspase-1 autoproteolysis is differentially required for NLRP1b and NLRP3 inflammasome function. *Proc. Natl. Acad. Sci. USA*. 111:17254-17259. <https://doi.org/10.1073/pnas.1415756111>
- Hagar, J.A., D.A. Powell, Y. Aachoui, R.K. Ernst, and E.A. Miao. 2013. Cytoplasmic LPS activates caspase-11: implications in TLR4-independent endotoxin shock. *Science*. 341:1250-1253. <https://doi.org/10.1126/science.1240988>
- Kajiwara, Y., T. Schiff, G. Voloudakis, M.A. Gama Sosa, G. Elder, O. Bozdagi, and J.D. Buxbaum. 2014. A critical role for human caspase-4 in endotoxin sensitivity. *J. Immunol.* 193:335-343. <https://doi.org/10.4049/jimmunol.1303424>
- Kang, T.B., G.S. Oh, E. Scandella, B. Bolinger, B. Ludewig, A. Kovalenko, and D. Wallach. 2008. Mutation of a self-processing site in caspase-8 compromises its apoptotic but not its nonapoptotic functions in bacterial artificial chromosome-transgenic mice. *J. Immunol.* 181:2522-2532. <https://doi.org/10.4049/jimmunol.181.4.2522>
- Kayagaki, N., S. Warming, M. Lamkanfi, L. Vande Walle, S. Louie, J. Dong, K. Newton, Y. Qu, J. Liu, S. Heldens, et al. 2011. Non-canonical inflammasome activation targets caspase-11. *Nature*. 479:117-121. <https://doi.org/10.1038/nature10558>
- Kayagaki, N., M.T. Wong, I.B. Stowe, S.R. Ramani, L.C. Gonzalez, S. Akashi-Takamura, K. Miyake, J. Zhang, W.P. Lee, A. Muszyński, et al. 2013. Non-canonical inflammasome activation by intracellular LPS independent of TLR4. *Science*. 341:1246-1249. <https://doi.org/10.1126/science.1240248>
- Kayagaki, N., I.B. Stowe, B.L. Lee, K. O'Rourke, K. Anderson, S. Warming, T. Cuellar, B. Haley, M. Roose-Girma, Q.T. Phung, et al. 2015. Caspase-11 cleaves gasdermin D for non-canonical inflammasome signalling. *Nature*. 526:666-671. <https://doi.org/10.1038/nature15541>
- Liu, X., Z. Zhang, J. Ruan, Y. Pan, V.G. Magupalli, H. Wu, and J. Lieberman. 2016. Inflammasome-activated gasdermin D causes pyroptosis by forming membrane pores. *Nature*. 535:153-158. <https://doi.org/10.1038/nature18629>
- Mariathasan, S., D.S. Weiss, K. Newton, J. McBride, K. O'Rourke, M. Roose-Girma, W.P. Lee, Y. Weinrauch, D.M. Monack, and V.M. Dixit. 2006. Cryopyrin activates the inflammasome in response to toxins and ATP. *Nature*. 440:228-232. <https://doi.org/10.1038/nature04515>
- Meixenberger, K., F. Pache, J. Eitel, B. Schmeck, S. Hippenstiel, H. Slevogt, P. N'Guessan, M. Witznath, M.G. Netea, T. Chakraborty, et al. 2010. Listeria monocytogenes-infected human peripheral blood mononuclear cells produce IL-1beta, depending on listeriolysin O and NLRP3. *J. Immunol.* 184:922-930. <https://doi.org/10.4049/jimmunol.0901346>
- Philip, N.H., A. DeLaney, L.W. Peterson, M. Santos-Marrero, J.T. Grier, Y. Sun, M.A. Wynosky-Dolfi, E.E. Zwack, B. Hu, T.M. Olsen, et al. 2016. Activity of Uncleaved Caspase-8 Controls Anti-bacterial Immune Defense and TLR-Induced Cytokine Production Independent of Cell Death. *PLoS Pathog.* 12:e1005910. <https://doi.org/10.1371/journal.ppat.1005910>
- Pilla, D.M., J.A. Hagar, A.K. Haldar, A.K. Mason, D. Degrandi, K. Pfeffer, R.K. Ernst, M. Yamamoto, E.A. Miao, and J. Coers. 2014. Guanylate binding proteins promote caspase-11-dependent pyroptosis in response to cytoplasmic LPS. *Proc. Natl. Acad. Sci. USA*. 111:6046-6051. <https://doi.org/10.1073/pnas.1321700111>
- Ramirez, M.L.G., M. Poreba, S.J. Snipas, K. Groborz, M. Drag, and G.S. Salvesen. 2018. Extensive peptide and natural protein substrate screens reveal that mouse caspase-11 has much narrower substrate specificity than caspase-1. *J. Biol. Chem.* 293:7058-7067. <https://doi.org/10.1074/jbc.RA117.001329>
- Rathinam, V.A., S.K. Vanaja, L. Waggoner, A. Sokolovska, C. Becker, L.M. Stuart, J.M. Leong, and K.A. Fitzgerald. 2012. TRIF licenses caspase-11-dependent NLRP3 inflammasome activation by gram-negative bacteria. *Cell*. 150:606-619. <https://doi.org/10.1016/j.cell.2012.07.007>
- Renatus, M., H.R. Stennicke, F.L. Scott, R.C. Liddington, and G.S. Salvesen. 2001. Dimer formation drives the activation of the cell death protease caspase 9. *Proc. Natl. Acad. Sci. USA*. 98:14250-14255. <https://doi.org/10.1073/pnas.231465798>
- Sagulenkov, V., N. Vitak, P.R. Vajjhala, J.E. Vince, and K.J. Stacey. 2018. Caspase-1 Is an Apical Caspase Leading to Caspase-3 Cleavage in the AIM2 Inflammasome Response, Independent of Caspase-8. *J. Mol. Biol.* 430:238-247. <https://doi.org/10.1016/j.jmb.2017.10.028>
- Sborgi, L., S. Rühl, E. Mulvihill, J. Pipercevic, R. Heilig, H. Stahlberg, C.J. Farady, D.J. Müller, P. Broz, and S. Hiller. 2016. GSDMD membrane pore formation constitutes the mechanism of pyroptotic cell death. *EMBO J.* 35:1766-1778. <https://doi.org/10.15252/embj.201694696>

- Shi, J., Y. Zhao, Y. Wang, W. Gao, J. Ding, P. Li, L. Hu, and F. Shao. 2014. Inflammatory caspases are innate immune receptors for intracellular LPS. *Nature*. 514:187–192. <https://doi.org/10.1038/nature13683>
- Shi, J., Y. Zhao, K. Wang, X. Shi, Y. Wang, H. Huang, Y. Zhuang, T. Cai, F. Wang, and F. Shao. 2015. Cleavage of GSDMD by inflammatory caspases determines pyroptotic cell death. *Nature*. 526:660–665. <https://doi.org/10.1038/nature15514>
- Sutterwala, F.S., L.A. Mijares, L. Li, Y. Ogura, B.I. Kazmierczak, and R.A. Flavell. 2007. Immune recognition of *Pseudomonas aeruginosa* mediated by the IPAF/NLRC4 inflammasome. *J. Exp. Med.* 204:3235–3245. <https://doi.org/10.1084/jem.20071239>
- Taabazuing, C.Y., M.C. Okondo, and D.A. Bachovchin. 2017. Pyroptosis and Apoptosis Pathways Engage in Bidirectional Crosstalk in Monocytes and Macrophages. *Cell Chem. Biol.* 24:507–514.e4. <https://doi.org/10.1016/j.chembiol.2017.03.009>
- Thornberry, N.A., H.G. Bull, J.R. Calaycay, K.T. Chapman, A.D. Howard, M.J. Kostura, D.K. Miller, S.M. Molineaux, J.R. Weidner, J. Aunins, et al. 1992. A novel heterodimeric cysteine protease is required for interleukin-1 beta processing in monocytes. *Nature*. 356:768–774. <https://doi.org/10.1038/356768a0>
- Van de Craen, M., W. Declercq, I. Van den brande, W. Fiers, and P. Vandenaebelle. 1999. The proteolytic procaspase activation network: an in vitro analysis. *Cell Death Differ.* 6:1117–1124. <https://doi.org/10.1038/sj.cdd.4400589>
- Walker, N.P., R.V. Talanian, K.D. Brady, L.C. Dang, N.J. Bump, C.R. Ferenz, S. Franklin, T. Ghayur, M.C. Hackett, L.D. Hammill, et al. 1994. Crystal structure of the cysteine protease interleukin-1 beta-converting enzyme: a (p20/p10)₂ homodimer. *Cell*. 78:343–352. [https://doi.org/10.1016/0092-8674\(94\)90303-4](https://doi.org/10.1016/0092-8674(94)90303-4)
- Walsh, J.G., S.E. Logue, A.U. Lüthi, and S.J. Martin. 2011. Caspase-1 promiscuity is counterbalanced by rapid inactivation of processed enzyme. *J. Biol. Chem.* 286:32513–32524. <https://doi.org/10.1074/jbc.M111.225862>
- Wang, S., M. Miura, Y. Jung, H. Zhu, V. Gagliardini, L. Shi, A.H. Greenberg, and J. Yuan. 1996. Identification and characterization of Ich-3, a member of the interleukin-1beta converting enzyme (ICE)/Ced-3 family and an upstream regulator of ICE. *J. Biol. Chem.* 271:20580–20587. <https://doi.org/10.1074/jbc.271.34.20580>
- Wang, S., M. Miura, Y.K. Jung, H. Zhu, E. Li, and J. Yuan. 1998. Murine caspase-11, an ICE-interacting protease, is essential for the activation of ICE. *Cell*. 92:501–509. [https://doi.org/10.1016/S0092-8674\(00\)80943-5](https://doi.org/10.1016/S0092-8674(00)80943-5)
- Yang, J., Y. Zhao, and F. Shao. 2015. Non-canonical activation of inflammatory caspases by cytosolic LPS in innate immunity. *Curr. Opin. Immunol.* 32:78–83. <https://doi.org/10.1016/j.coi.2015.01.007>